Journal of Power Sources 229 (2013) 95–101

Contents lists available at SciVerse ScienceDirect

Journal of Power Sources

journal homepage: www.elsevier.com/locate/jpowsour

Chemically stable and easily sintered high-temperature proton conductor $BaZr_{0.8}In_{0.2}O_{3-\delta}$ for solid oxide fuel cells

Wenping Sun [a,c], Zhiwen Zhu [a], Zhen Shi [a], Wei Liu [a,b,*]

[a] CAS Key Laboratory of Materials for Energy Conversion, Department of Materials Science and Engineering, University of Science and Technology of China (USTC), Hefei 230026, PR China
[b] Key Laboratory of Materials Physics, Institute of Solid State Physics, Chinese Academy of Sciences, Hefei 230031, PR China
[c] School of Materials Science and Engineering, Georgia Institute of Technology, 771 Ferst Drive, Atlanta, GA 30332, USA

HIGHLIGHTS

- $BaZr_{0.8}In_{0.2}O_{3-\delta}$ (BZI) powders were synthesized via the gel combustion process.
- BZI shows good sintering activity and high chemical stability.
- The electrical conductivity of dense BZI pellet was investigated in detail.
- A single cell with a dense BZI electrolyte film was fabricated and tested.

ARTICLE INFO

Article history:
Received 4 October 2012
Received in revised form
1 December 2012
Accepted 3 December 2012
Available online 12 December 2012

Keywords:
Acceptor-doped barium zirconate
High-temperature proton conductor
Electrical conductivity
Electrochemical impedance spectroscopy
Proton-conducting solid oxide fuel cells

ABSTRACT

Barium zirconate-based high-temperature proton conductors (HTPCs) exhibit excellent chemical stability in atmospheres containing CO_2 or water vapor. However, such HPTCs haven't been widely used as electrolyte materials for solid oxide fuel cells (SOFCs) due to their poor sintering activity. In this work, indium is selected as a dopant to improve the sintering activity of barium zirconate. $BaZr_{0.8}In_{0.2}O_{3-\delta}$ (BZI) powders with a pure cubic perovskite structure are synthesized via a typical citric acid–nitrate gel combustion process. The SEM results show that BZI exhibits improved sintering activity compared to the state-of-the-art proton conductor $BaZr_{0.8}Y_{0.2}O_{3-\delta}$ (BZY), and fully dense BZI pellets with increased grain size are obtained after sintered at 1600 °C in air. Moreover, BZI also keeps sufficiently high chemical stability as BZY. The electrical conductivity of BZI under various atmospheres is investigated by electrochemical impedance spectroscopy (EIS) in detail. The total conductivity achieves 1.0×10^{-3} S cm^{-1} at 700 °C in wet H_2 (3% H_2O). Dense BZI electrolyte films are successfully fabricated on the anode substrates by a dry-pressing method after sintered at 1400 °C for 5 h in air. Single cells with dense BZI electrolyte films are also assembled and tested to further evaluate the feasibility of BZI as an electrolyte material for proton-conducting SOFCs.

1. Introduction

High-temperature proton conductors (HTPCs) have been extensively investigated worldwide since Iwahara and co-workers reported proton conduction in some perovskite-type materials under atmospheres containing water vapor or H_2 at elevated temperatures [1–4]. Nowadays, HTPCs are widely applied to solid oxide fuel cells (SOFCs) [5,6], hydrogen separation membranes [7], hydrogen sensors [8], and steam electrolysers [9]. Especially, HTPCs are considered to be the most promising electrolyte materials for intermediate/low-temperature SOFCs due to their excellent ionic conductivity at reduced temperatures [5].

Although a variety of materials with various crystal structures have been found to exhibit proton conduction, acceptor-doped $BaCeO_3$ and $BaZrO_3$ compounds are the most well-known HTPCs [4–6,10–15]. Acceptor-doped $BaCeO_3$ is known for the high proton conductivity; however, $BaCeO_3$ is not chemically stable at all under atmospheres containing CO_2 or water vapor [10,16,17]. Acceptor-doped $BaZrO_3$ shows excellent chemical stability; however, it is not very easy to fabricate dense pellets or membranes for electrochemical devices because of its poor sintering ability [12,13]. In order to make a balance between chemical stability and proton conductivity, $BaCeO_3$–$BaZrO_3$ solid solution was developed and

* Corresponding author. CAS Key Laboratory of Materials for Energy Conversion, Department of Materials Science and Engineering, University of Science and Technology of China (USTC), Hefei 230026, PR China. Tel.: +86 (0)551 3606929; fax: +86 (0)551 3602586.
E-mail address: wliu@ustc.edu.cn (W. Liu).

0378-7753/$ – see front matter © 2012 Elsevier B.V. All rights reserved.
http://dx.doi.org/10.1016/j.jpowsour.2012.12.017

investigated [5,6,10]. As expected, $BaCeO_3$–$BaZrO_3$ solid solution exhibits adequate proton conductivity and acceptable chemical stability. In addition to Zr, some other dopants, such as Ta [18], In [19,20], Nb [21], Ti [22], and Ga [23], were introduced to the Ce-site of $BaCeO_3$ to improve the chemical stability of $BaCeO_3$-based HTPCs. After substitution, the chemical stability was improved to some extent at the expense of proton conductivity. However, it must be mentioned that the modified $BaCeO_3$-based proton conductors still decompose when they are exposed to atmospheres containing slightly high concentrations of CO_2 or water vapor [15,17]. Therefore, given the unsatisfying chemical stability, $BaCeO_3$-based HTPCs cannot meet the demands of practical applications. Compared to $BaCeO_3$, acceptor-doped $BaZrO_3$ displays substantial chemical stability against CO_2 and water vapor [13,15]. From the stability point of view, $BaZrO_3$-based oxides are the most promising proton conductors for practical applications. In our opinion, more research attention should be focused on promoting sintering activity and electrical conductivity of $BaZrO_3$-based HTPCs. In most cases, sintering aids, such as ZnO [12], NiO [24], and CuO [25], were used to enhance the sintering activity of $BaZrO_3$-based HTPCs. Recently, it was reported that some dopants might also help to reduce the sintering temperature of perovskite oxides, such as In [19,20,26,27] and Pr [15,28,29]. Bi et al. [19] employed In as a dopant to $BaCeO_3$, and they found that the $BaCe_{0.7}In_{0.3}O_{3-\delta}$ membrane got dense after sintered at a low temperature of 1100 °C. Similar results were observed in $BaZrO_3$. Naoki et al. [26] reported that the sintering ability of $BaZr_{0.9}Y_{0.1}O_{3-\delta}$ was enhanced after co-doped with In. Pr isn't a proper dopant if the proton conductor is used as the electrolyte for SOFCs because the multivalent character of Pr would induce *n*-type electrical conduction under reducing atmospheres at elevated temperatures [29]. The *n*-type electrical conduction would cause internal short circuit of the fuel cell.

In this work, we selected In as the dopant for $BaZrO_3$, and $BaZr_{0.8}In_{0.2}O_{3-\delta}$ (BZI) was synthesized and evaluated as the electrolyte material for proton-conducting SOFCs. The sintering activity, chemical stability and electrical conductivity of BZI under various atmospheres were investigated in detail. Anode-supported single cells with dense BZI electrolyte films were also fabricated and tested to evaluate the possibility of BZI as a proton-conducting electrolyte material.

2. Experimental

2.1. Powder synthesis

$BaZr_{0.8}In_{0.2}O_{3-\delta}$ (BZI) powders were synthesized via a typical citric acid–nitrate gel combustion process [30]. Firstly, $Zr(NO_3)_4 \cdot 5H_2O$ and $In(NO_3)_4 \cdot 4.5H_2O$ were dissolved in deionized water with stirring and heating on a hot plate. After the solution got clear, $Ba(CH_3COO)_2$ was then added. Citric acid was added in metal ions: citric acid molar ratio of 1:1.5 and the pH value was adjusted to about 7 with $NH_3 \cdot H_2O$. The solution was heated and stirred continuously at about 70 °C until gelling. After a while, gel ignition and combustion occurred, yielding the as-prepared black powders. Finally, the black powders were calcined at 1100 °C for 6 h in air to form BZI powders a pure perovskite phase. For comparison, $BaZr_{0.8}Y_{0.2}O_{3-\delta}$ (BZY) powders were also prepared via the same procedure.

2.2. Characterization and electrochemical measurement

To evaluate the chemical stability of BZI, BZI powders were treated in wet 3% CO_2 (balanced with air, 3% H_2O) for 10 h and wet CO_2 (3% H_2O) for 24 h, respectively, and BZI dense pellet was treated in boiling water for 4 h and 12 h, respectively.

The BZI pellets used for electrical conductivity measurement were sintered at 1600 °C for 24 h. The total electrical conductivity of the sintered BZI pellet in various atmospheres was studied via a two-point method using an impedance analyzer (CHI604B, Chenhua Inc., Shanghai) with an amplitude of 5 mV in the frequency range from 100 kHz to 0.1 Hz. Pt paste was brush-painted symmetrically on both sides of the sintered BZI pellet as current collectors and then fired at 950 °C for 1 h to remove the residual organics and attain good adhesion between the pellet and Pt layer. Dry gas was obtained after passing through 98% H_2SO_4. Wet gas was achieved after flowing through a bubbling bottle at a given temperature, and the saturation vapor pressure at the given temperature was just the water vapor partial pressure. The measurement was repeated several times at each temperature until the resistances became constant from one measurement to the next.

The green BZI films were deposited on the anode substrates by a dry-pressing method [30]. $BaZr_{0.1}Ce_{0.7}Y_{0.2}O_{3-\delta}$ and NiO mixed in a weight ratio of 40:60 was used for preparing anode substrates. The green anode-supported BZI films were fired at 1400 °C for 5 h to get dense and ultimately obtain BZI-based half cells. $Sm_{0.5}Sr_{0.5}CoO_{3-\delta}$–$Ce_{0.8}Sm_{0.2}O_{2-\delta}$ (SSC–SDC) composite cathode slurry was brush-painted onto the BZI electrolyte film and then fired at 950 °C for 3 h in air to form a porous cathode layer. Single cells were tested from 600 to 700 °C with humidified hydrogen (2% H_2O) as the fuel and static air as the oxidant, respectively. The flow rate of the fuel gas was about 30 mL min^{-1}. The cell performance was measured with a DC Electronic Load (ITech Electronics model IT8511). Electrochemical impedance spectra of the cell under open circuit conditions were measured using an impedance analyzer (CHI604B, Chenhua Inc., Shanghai) with an amplitude of 5 mV in the frequency range from 100 kHz to 0.1 Hz. The spectrum curve fitting was performed using the ZSimpWin Software.

Phase structures of the powders and pellets were identified by an X-ray diffractometer (Rigaku TTR-III) using CuKα radiation. The microstructure of the sintered pellets and the tested cell was examined by SEM (JEOL JSM-6700F).

3. Results and discussion

3.1. Phase structure

Fig. 1 shows the XRD pattern of the BZI powders calcined at 1100 °C for 6 h in air. Indexing of the pattern clearly indicates that

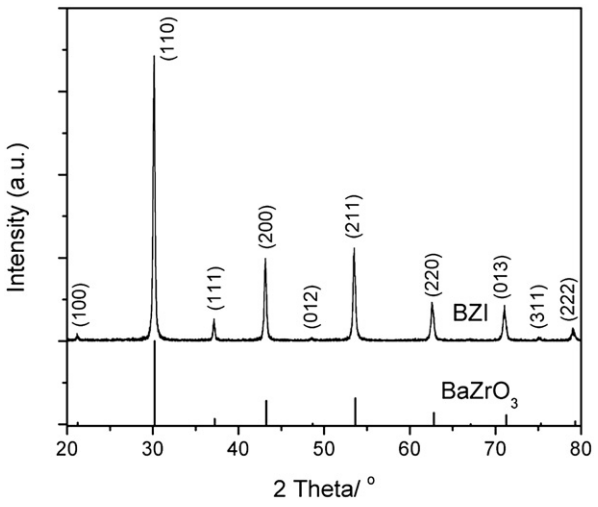

Fig. 1. XRD pattern of the BZI powders calcined at 1100 °C for 6 h in air.

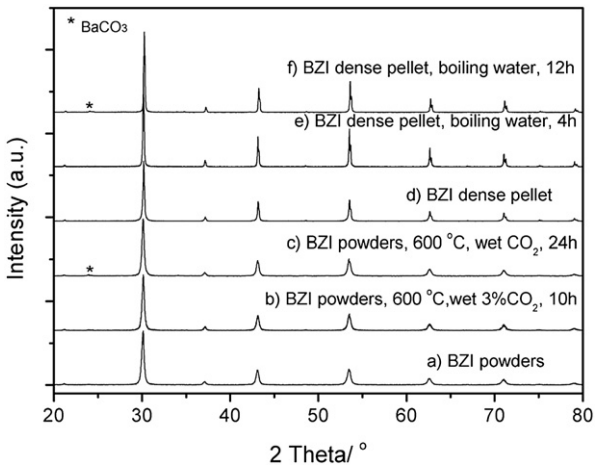

Fig. 2. XRD patterns of: a–c) BZI powders before (a), and after exposure to wet 3% CO_2 at 600 °C for 10 h (b), and to wet CO_2 (3% H_2O) at 600 °C for 24 h (c); d–f) BZI pellet before (d), and after exposure to boiling water for 4 h (e) and 12 h (f).

BZI has a cubic symmetry of space group *Pm-3m*. The Goldschmidt tolerance factor of BZI is calculated to be 0.996, which is very close to unity, and this also confirms the cubic structure of BZI. Compared to the XRD pattern of the un-doped cubic barium zirconate, the characteristic peaks of BZI shift toward lower reflection angles. The shifting is in accordance with the ionic radius variation that In^{3+} (6-coordination with oxygen, 0.80 Å) has a larger radius than Zr^{4+} (6-coordination with oxygen, 0.72 Å) [31]. The XRD result also reveals that the unit cell volume increases after incorporating indium into the zirconium site.

3.2. Chemical stability

To evaluate the chemical stability against CO_2 and water vapor, BZI powders and dense pellets were treated in atmospheres containing H_2O or CO_2, even in boiling water and wet CO_2 (3% H_2O). Fig. 2 shows the XRD patterns of BZI powders and pellets after chemical stability test. As can be seen, the pattern of BZI powders remains unchanged after exposed to a wet atmosphere containing 3% CO_2 at 600 °C for 10 h, and no other phases were formed when the BZI pellet was treated in boiling water for 4 h. The results suggest that BZI is indeed much more chemically stable than those $BaCeO_3$-based proton conductors, which can be easily corroded by CO_2 or water vapor [10,16,17]. However, a very weak peak corresponding to barium carbonate was observed in the XRD pattern when BZI powders were exposed in wet CO_2 (3% H_2O) at 600 °C for 24 h, implying that the reaction between $BaZrO_3$ and CO_2 occurred in such a terrible environment. As a matter of fact, $BaZrO_3$ isn't totally thermodynamically stable against CO_2 [32]. When $BaZrO_3$ is exposed in an atmosphere containing sufficiently high concentration of CO_2, it will react with CO_2, thus forming barium carbonate and zirconium oxide. Moreover, very small amounts of barium carbonate were also detected after BZI pellet was treated in boiling water for a longer time of 12 h. Anyway, BZI is a very promising stable proton conductor as compared to $BaCeO_3$-based oxides.

3.3. Sintering activity

To date, $BaZrO_3$-based HTPCs haven't been widely used as electrolytes for SOFCs due to the poor sintering activity. It's expected that the sintering activity of $BaZrO_3$ can be enhanced after incorporating In instead of Y into B-site as a dopant. SEM images of the

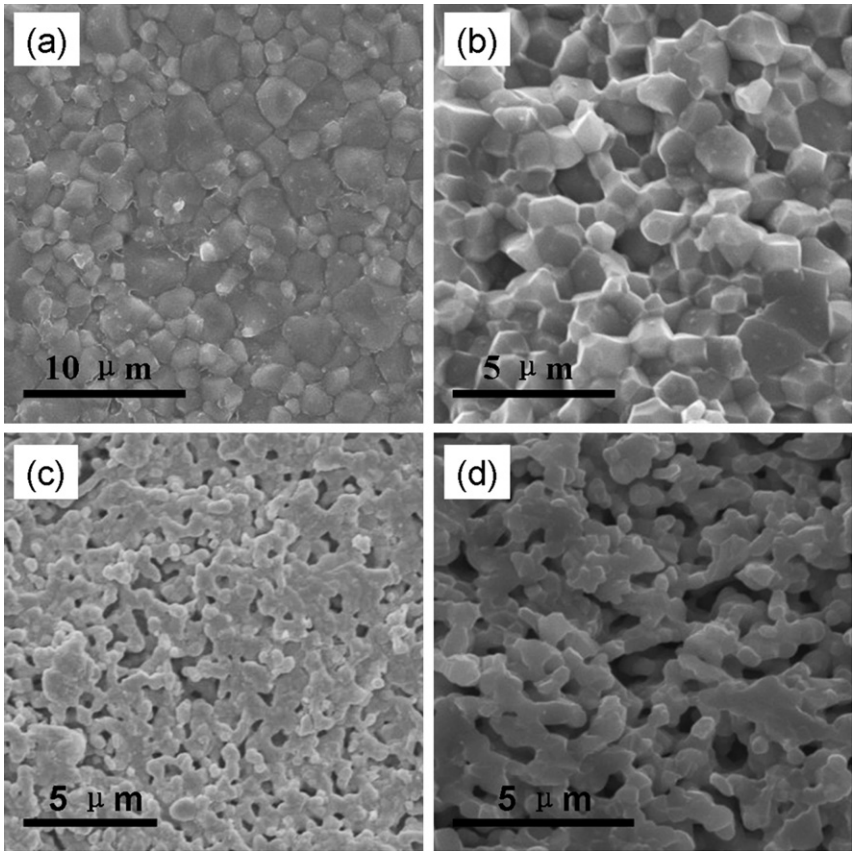

Fig. 3. SEM images of the surface and cross-section fracture of the sintered BZI (a, b) and BZY (c, d) pellets.

surface and cross-section fracture of the BZI and BZY pellets sintered at 1600 °C for 24 h are shown in Fig. 3. It can be seen that the BZI pellet is nearly fully dense, and only a few closed pores can be found in the fracture (Fig. 3(a) and (b)). The relative density of the BZI pellet was also estimated via the typical Archimedes method, achieving as high as 99%, which is completely in consistent with the SEM results. In contrast with BZI, BZY is still very porous and the relative density is only about 84% (Fig. 3(c) and (d)). The relative density and morphology variation of the sintered pellets reveals that In can substantially improve the sintering activity of $BaZrO_3$. The dense pellet ensures that the measured conductivity could reflect the intrinsic transport behavior of BZI, much better than those porous samples. Moreover, the grain size of BZI pellet is about 2−3 μm and remarkably improved compared to the BZY pellet, the grain size of which was even less than 1 μm. Larger grain size means lower grain boundary density and is beneficial for decreasing grain boundary resistance for $BaZrO_3$-based proton conductors [12,14,33]. The internal reason for sintering enhancement is till unclear to us. The improved sintering activity of BZI might be partially caused by the low melting point of indium oxide, which might help to form a liquid phase to serve as a sintering aid during sintering [26]. The sintering process is very complicated and more work needs to be done to further understand the detailed mechanism.

3.4. Conductivity

As is known, the ohmic resistance of a single cell is dominated by the electrolyte resistance. Thus, it is critical to investigate the electrical conductivity of BZI to evaluate the feasibility as a proton-conducting electrolyte for SOFCs. The electrical conductivity of the sintered dense BZI pellet was measured under various atmospheres using AC electrochemical impedance spectroscopy (EIS). Fig. 4 shows the typical EIS curves of the BZI pellet measured in dry O_2 from 150 to 400 °C. At 150 °C, the spectroscopy displays three obvious arcs (Fig. 4(a)). The high-frequency arc (arc 1) clearly extends to the origin, and the capacitance of the high-frequency arc is estimated to be about 4.1×10^{-11} F cm^{-2}, typical of a bulk response here. The mid-frequency arc (arc 2) should be attributed to the grain boundary response, and the capacitance is about 5.9×10^{-9} F cm^{-2}. And, the low-frequency arc (arc 3) is corresponding to the electrode process. As the temperature increases, the high-frequency arc gradually becomes inaccessible and finally

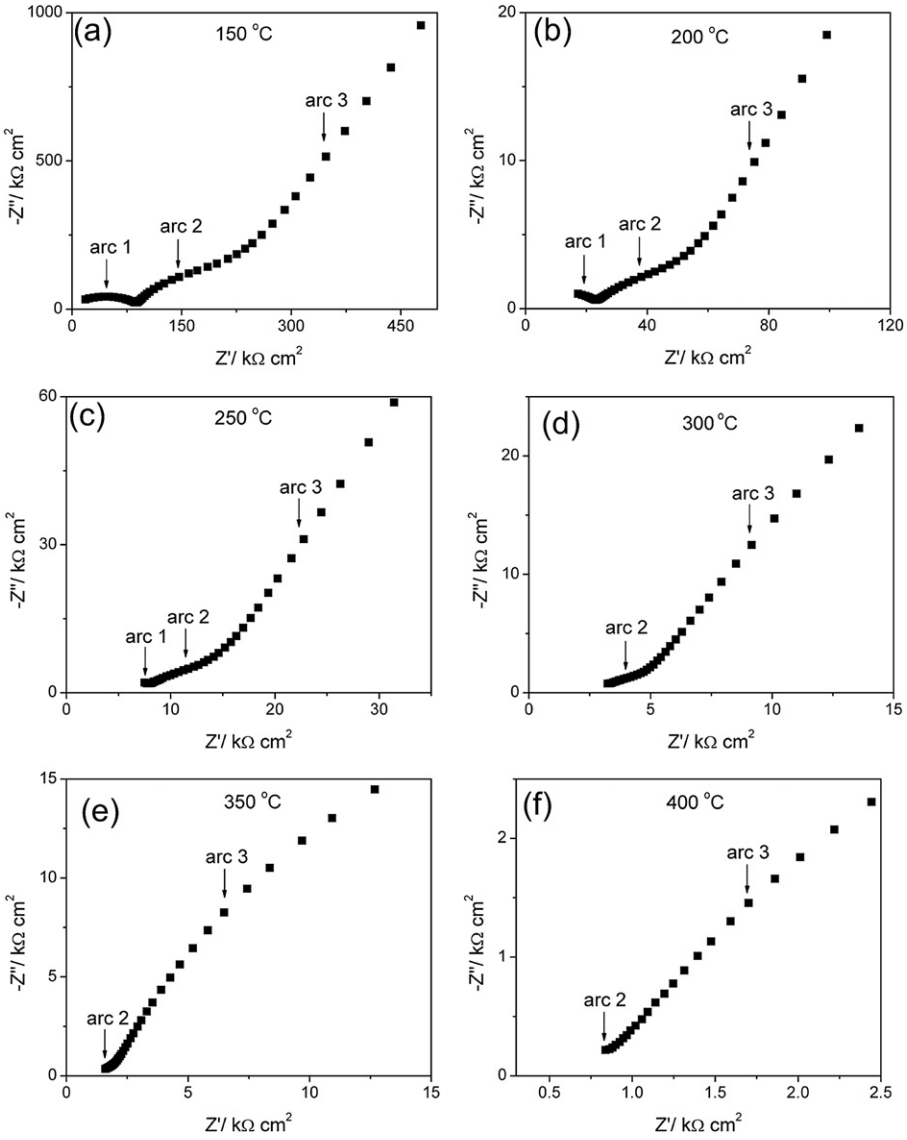

Fig. 4. Electrochemical impedance spectra of BZI pellet obtained in dry O_2 at the noted temperature (a) 150 °C, (b) 200 °C, (c) 250 °C, (d) 300 °C, (e) 350 °C, (f) 400 °C.

disappears at temperatures higher than 300 °C (Fig. 4(b)–(d)). Furthermore, the bulk and grain boundary contributions to the total resistance cannot be separated at all when the temperature is higher than 350 °C (Fig. 4(e) and (f)). In these cases, the spectra are mainly associated with the electrode process and only the total resistances can be estimated from the spectra.

The temperature dependence of the total electrical conductivity of BZI dense pellet under different atmospheres is shown in Fig. 5. A notable difference in the conductivity of the sample measured in wet (3% H_2O) and dry O_2 can be observed (Fig. 5(a)). The conductivity in dry O_2 is higher than that in wet O_2 (3% H_2O) at temperatures higher than 500 °C, and this should be attributed to the electron-hole conduction, as shown in Eq. (1),

$$\frac{1}{2}O_2(g) + V_O^{\cdot\cdot} \rightarrow O_O^{\times} + 2h^{\cdot} \quad (1)$$

Electron-hole conduction is the dominating mechanism for $BaZrO_3$-based proton conductors in a dry atmosphere with a high oxygen partial pressure, and oxygen-ion conduction contributes very few to the total conductivity under such atmospheres [11].

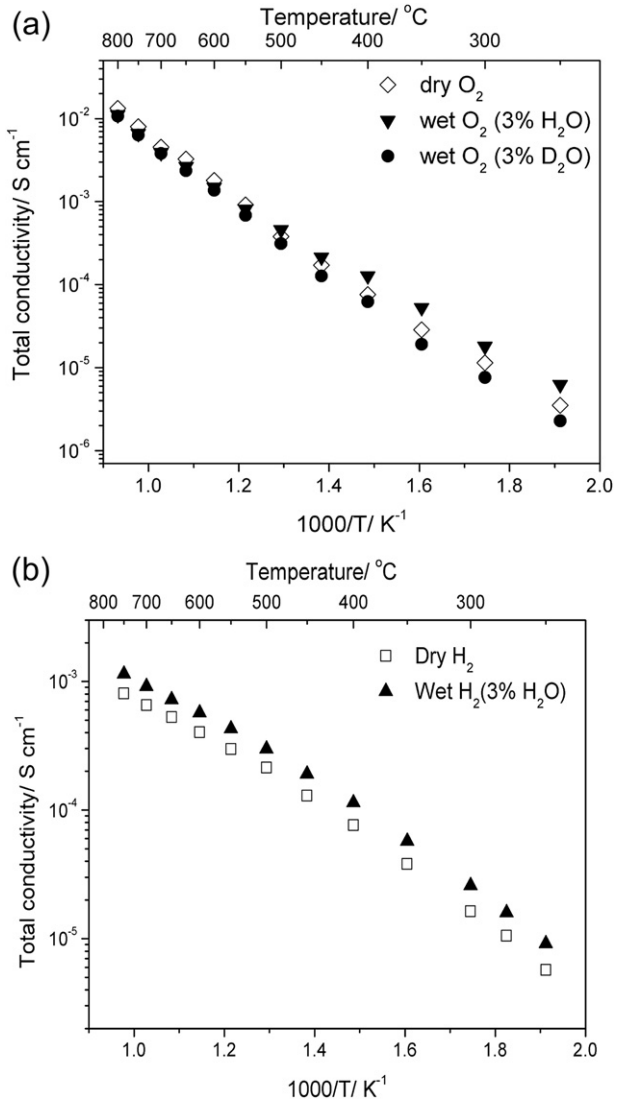

Fig. 5. The total electrical conductivity of BZI pellet measured in oxygen (a) and hydrogen (b).

While, the conductivity in wet O_2 (3% H_2O) is superior at temperatures lower than 500 °C. Herein proton conduction should response for the conductivity enhancement, according to Eq. (2),

$$H_2O(g) + O_O^{\times} + V_O^{\cdot\cdot} \rightarrow 2(OH)_O^{\cdot} \quad (2)$$

Notably, for proton-conducting oxides, the hydration reaction is exothermic, and hence the proton concentration in the oxides increases with decreasing the temperature. Thus, as the temperature decreases, proton conduction gradually plays a more and more important role. At the same time, according to Eqs. (1) and (2), the electron–hole conduction is partially suppressed after introducing water vapor into the atmosphere. The apparent activation energy E_a for the conductivity in dry O_2 is calculated to be 0.80 eV, while the E_a value decreases to 0.71 eV in wet O_2 (3% H_2O). The reduction of E_a value also indicates the presence of proton conduction in wet environment. The proton conduction was also verified by the H/D isotope effect, which is most commonly used to determine if a conductor is proton-conducting or not. Ideally, if the charge carriers are all protons or deuterons, the isotope effect expected for the conductivity measurement is that $\sigma_H/\sigma_D \approx \sqrt{2}$ [34,35]. As can be seen from Fig. 5(a), the conductivity in O_2 (3% H_2O) is higher than that in O_2 (3% D_2O), especially at lower temperatures. The conductivity ratio $\sigma(H_2O)/\sigma(D_2O)$ ranges between 1.4 and 2.7 at temperatures lower than 500 °C, and similar results were also attained in some other proton-conducting oxides [15,35]. The ratio deviation might indicate the non-classical proton hopping. Besides, the ratio is around unity at temperatures higher than 500 °C, which is consistent with the fact that proton defect is more stable and proton conduction contributes more at lower temperatures. At 500 °C, the total electrical conductivity of BZI is 3.80×10^{-4}, 4.57×10^{-4}, and 3.11×10^{-4} S cm^{-1} in dry O_2, O_2 (3% H_2O) and O_2 (3% D_2O), respectively. The conductivity in hydrogen atmospheres was also evaluated, as shown in Fig. 5(b). The conductivity in wet H_2 is significantly higher than that in dry H_2, suggesting that proton conduction is enhanced in the presence of water vapor. In dry H_2, hydrogen molecules firstly dissociate; then, the protons will be attached to the oxygen ion sites forming hydroxide ions, as shown in Eq. (3),

$$H_2 + 2O_O^{\times} \rightarrow 2OH_O^{\cdot} + 2e^{'} \quad (3)$$

Protons can also be incorporated into BZI via Eq. (2) after water vapor is introduced. Consequently, proton concentration in BZI increases significantly with the help of water vapor and correspondingly the proton conductivity is improved. The total conductivity in dry H_2 is 6.5×10^{-4} S cm^{-1} at 700 °C, while the value increases to about 1.0×10^{-3} S cm^{-1} in wet H_2. The apparent activation energy E_a is calculated to be 0.52 and 0.50 eV in dry and wet H_2, respectively, which are in accordance with the values reported in the literature [15,32]. Notably, E_a is very close in dry and wet H_2, indicating that the proton transport mechanism is entirely identical in 2 atm. It has to be mentioned that the total conductivity of BZI in wet H_2 is smaller than the reported values of those well-sintered BZY samples [14,33]. Actually, the hydration behavior and mobility of proton defects in $BaZrO_3$ are very sensitive to the dopant. As reported by Kreuer [36], the hydration behavior and proton mobility of In-doped $BaZrO_3$ is not as good as Y-doped $BaZrO_3$. Therefore, to make a balance between sintering activity and proton conductivity of acceptor-doped $BaZrO_3$, In and Y co-doped $BaZrO_3$ might be a better choice.

3.5. SOFC applications

Fabricating dense $BaZrO_3$-based electrolyte films on porous anode substrates via the conventional ceramic process is still

a considerable challenge for proton-conducting SOFCs to date. In order to evaluate BZI as an electrolyte for SOFCs, anode-supported dense BZI electrolyte films were successfully fabricated by a dry-pressing technique followed by co-firing at 1400 °C for 5 h. Single cells with thin BZI electrolyte films were also assembled and tested. Fig. 6 shows SEM images of the cross section of the anode-supported BZI electrolyte film. Clearly, the electrolyte film is fully dense and crack-free, and even no pores can be observed. In contrast, some pores are still present in the BZY electrolyte film prepared via the similar procedure [30]. The comparison further confirms the good sintering activity of BZI. Additionally, the BZI film is about 20 μm in thickness and adhered firmly to the anode substrate. Fig. 7(a) shows the *I–V* and power density curves of the single cell. The peak power densities reach 85, 56, and 34 mW cm^{-2} at 700, 650, and 600 °C, respectively. The power densities are several times higher than those cells supported by acceptor-doped $BaZrO_3$ electrolytes, the peak power densities of which are only several mW cm^{-2}, even at the operating temperature as high as 800 °C [37–39]. Therefore, fabricating thin and dense electrolyte film is critical for outputting excellent cell performance. In addition, the power performance also shows obvious superiority to those fuel cells based on acceptor-doped $BaZrO_3$ thin films employing sintering aids. Peng et al. [39] reported a 10-μm-thick BZY-based cell with ZnO as sintering aid and the cell showed peak power density of 25 mW cm^{-2} at 800 °C. Sun et al. [40] used $LiNO_3$ to improve the sintering activity of BZY and the cell with a 25-μm-thick electrolyte film output peak power density of 53 mW cm^{-2} at 700 °C. Especially, the open circuit voltages (OCVs) of this BZI-based cell achieve 0.95, 0.98, and 1.01 V at 700, 650, and 600 °C, respectively, further confirming that the electrolyte film is dense enough to prevent gas leakage. The OCVs of this cell are higher than some other $BaZrO_3$-based fuel cells reported in literature [15,41]. Moreover, the OCVs are also comparable with those $BaCeO_3$-based proton-conducting SOFCs [5,6,19,21]. Further, the chemical stability of BZI electrolyte film under fuel cell conditions was also evaluated, as shown in Fig. 7(b). The OCV of the cell still kept stable after operating at 600 °C for about 32 h, indicating that the BZI electrolyte film was not broken at all after operating for 32 h under open circuit condition. If the BZI film reacts with water vapor or CO_2 coming from the fuel gas and air, the film will gradually decompose. In this case, gas leakage would occur and the OCV value would drop down correspondingly. The preliminary results demonstrate that BZI might be an appropriate electrolyte material for SOFCs.

Although fully dense BZI films on porous anode substrates have been successfully fabricated, the cell performance is still much

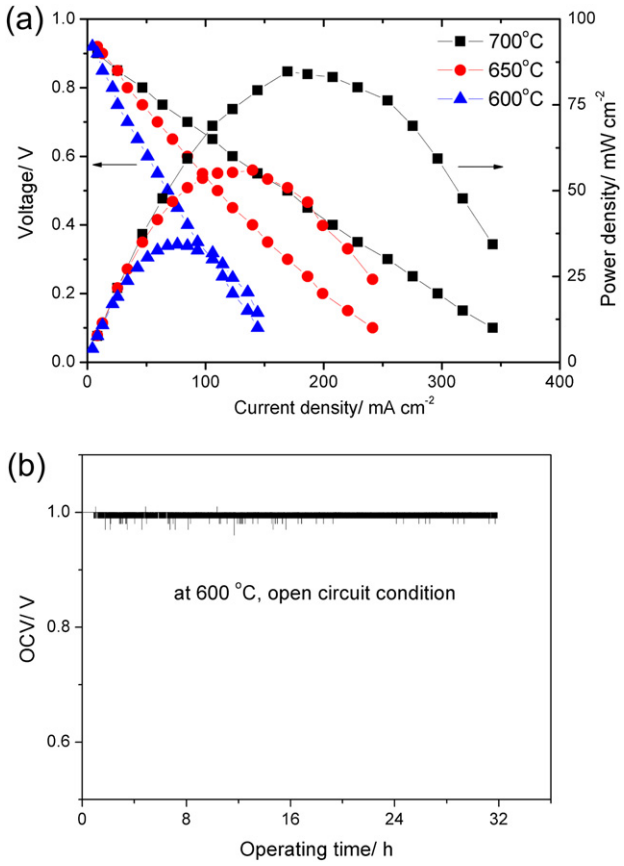

Fig. 7. (a) *I–V* and power density curves of BZI-based single cell with wet hydrogen (2% H_2O) as the fuel and static air as the oxidant. (b) Short-term stability of the OCV of BZI-based single cell at 600 °C.

lower than those state-of-the-art $BaCeO_3$-based proton-conducting SOFCs. To further investigate the intrinsic reasons for the unsatisfactory performance, electrochemical impedance spectra of the cell at different operating temperatures were measured under open circuit conditions, as shown in Fig. 8(a). In the spectra, the intercept with the real axis at high frequencies represents the ohmic resistance (R_{ohm}) of the cell, which is dominated by the resistance of the electrolyte membrane, and the difference between the high frequency and the low frequency intercept with the real axis

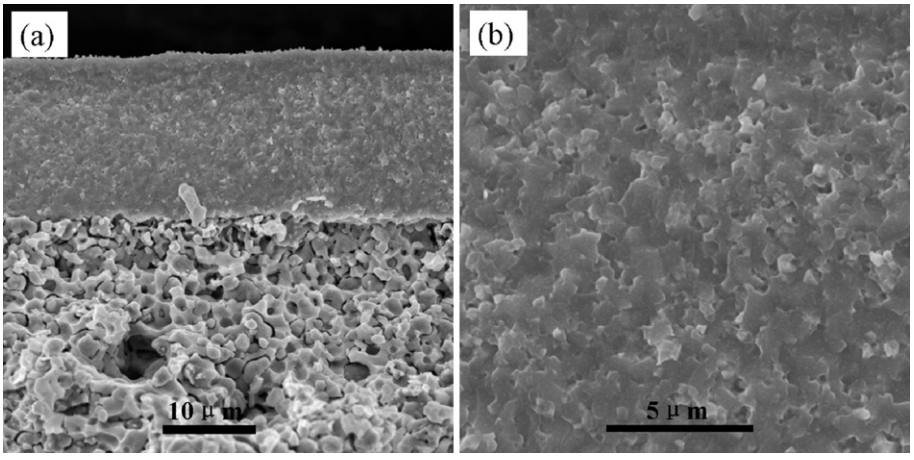

Fig. 6. SEM images of the cross section of the anode-supported half cell (a) and BZI electrolyte film (b).

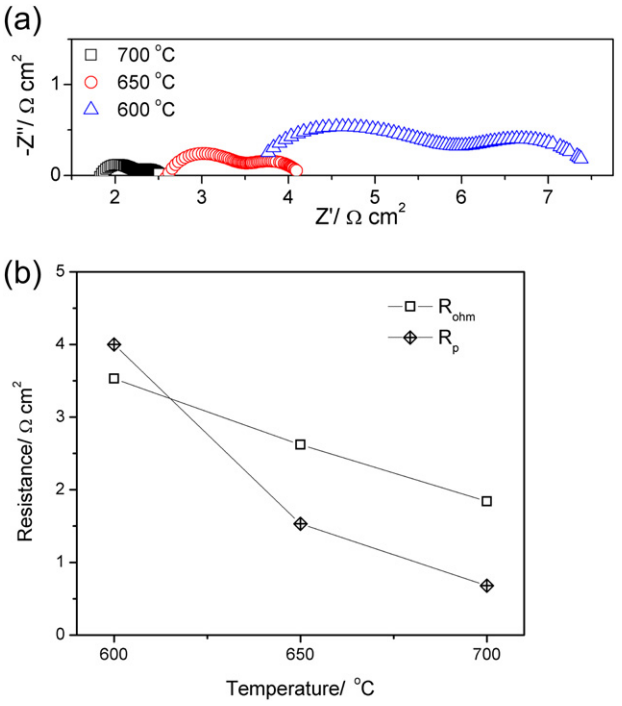

Fig. 8. (a) Electrochemical impedance spectra of the single cell measured under open circuit conditions. (b) The estimated ohmic resistances (R_{ohm}) and polarization resistances (R_p) of the cell determined from EIS under open circuit conditions.

represents the polarization resistance (R_p) of the cell, which is mainly determined by the electrode materials and microstructures. Obviously, both R_{ohm} and R_p dramatically increase as the operating temperature decreases. Fig. 8(b) shows the estimated R_{ohm} and R_p values of the tested cell. R_{ohm} is 1.84, 2.62, and 3.53 Ω cm^2, and R_p is 0.68, 1.53, and 4 Ω cm^2 at 700, 650, and 600 °C, respectively. Both R_{ohm} and R_p are much higher than the values of those high performance $BaCeO_3$-based cells [5,6]. That is to say, the power performance of the BZI-based cell is limited by the high R_{ohm} and R_p values. The high R_{ohm} results from the relatively low conductivity of BZI. Meanwhile, the high R_p is correlated with the electrode materials and microstructures of the cell. As can be seen from Fig. 6, the anode appears to be over densified and very few pores exist, which is detrimental to the fuel transportation. Moreover, the SSC–SDC cathode used in this work is easy to peel off the BZI electrolyte film and isn't a good cathode candidate for BZI electrolyte. The poor cathode/electrolyte interface would hinder charge transfer and current collecting, thus inducing high cell resistance. Therefore, in addition to highly conductive thin electrolyte film, highly active electrode materials and optimized microstructures are also essential for further improving the power performance of the BZI-based fuel cell.

4. Conclusions

In summary, $BaZr_{0.8}In_{0.2}O_{3-\delta}$ (BZI) was synthesized and evaluated as an electrolyte material for proton-conducting solid oxide fuel cells (SOFCs). BZI shows not only better sintering activity than $BaZr_{0.8}Y_{0.2}O_{3-\delta}$ (BZY) but also sufficiently high chemical stability. The total electrical conductivity of BZI is significantly dependent on the surrounding atmosphere, and achieves 1.0×10^{-3} S cm^{-1} at 700 °C in wet H_2. A 20-μm-thick dense BZI electrolyte film was fabricated and the corresponding single cell output acceptable power performance. All in all, indium turns out to be a good dopant for exploring sintering-active and stable $BaZrO_3$-based proton conductors. Nevertheless, the conductivity of BZI isn't high enough to meet the demands of low-temperature proton-conducting SOFCs. In order to make a balance between sintering activity and electrical conductivity, indium and yttrium co-doped $BaZrO_3$ might be a promising electrolyte material for low-temperature SOFCs.

Acknowledgments

This work was supported by the Natural Science Foundation of China (Grant No. 21076204) and the Ministry of Science and Technology of China (Grant No. 2012CB215403).

References

[1] H. Iwahara, T. Esaka, H. Uchida, N. Maeda, Solid State Ionics 3–4 (1981) 359–363.
[2] H. Iwahara, T. Yajima, T. Hibino, K. Ozaki, H. Suzuki, Solid State Ionics 61 (1993) 65–69.
[3] H. Iwahara, T. Yajima, H. Ushida, Solid State Ionics 70–71 (1994) 267–271.
[4] K.D. Kreuer, Annu. Rev. Mater. Res. 33 (2003) 333–359.
[5] C.D. Zuo, S.W. Zha, M.L. Liu, M. Hatano, M. Uchiyama, Adv. Mater. 18 (2006) 3318–3320.
[6] L. Yang, S.Z. Wang, K. Blinn, M.F. Liu, Z. Liu, Z. Cheng, M.L. Liu, Science 326 (2009) 126–129.
[7] C.D. Zuo, T.H. Lee, S.E. Dorris, U. Balachandran, M.L. Liu, Chem. Mater. 18 (2006) 4647–4650.
[8] T. Yajima, H. Iwahara, K. Koide, K. Yamamoto, Sens. Actuators B-Chem. 5 (1991) 145–147.
[9] F. He, D. Song, R.R. Peng, G.Y. Meng, S.F. Yang, J. Power Sources 195 (11) (2010) 3359–3364.
[10] K.H. Ryu, S.M. Haile, Solid State Ionics 125 (1999) 355–367.
[11] H.G. Bohn, T. Schober, J. Am. Ceram. Soc. 83 (2000) 768–772.
[12] P. Babilo, S.M. Haile, J. Am. Ceram. Soc. 88 (9) (2005) 2362–2368.
[13] S.W. Tao, J.T.S. Irvine, Adv. Mater. 18 (2006) 1581–1584.
[14] Y. Yamazaki, R. Hernandez-Sanchez, S.M. Haile, Chem. Mater. 21 (2009) 2755–2762.
[15] E. Fabbri, L. Bi, H. Tanaka, D. Pergolesi, E. Traversa, Adv. Funct. Mater. 21 (2011) 158–166.
[16] F.L. Chen, O.T. Sørensen, G.Y. Meng, D.K. Peng, J. Mater. Chem. 7 (1997) 481–485.
[17] C.S. Tu, R.R. Chien, V.H. Schmidt, S.C. Lee, C.C. Huang, C.L. Tsai, J. Appl. Phys. 105 (2009) 103504 (1–7).
[18] L. Bi, S.Q. Zhang, S.M. Fang, Z.T. Tao, R.R. Peng, W. Liu, Electrochem. Commun. 10 (10) (2008) 1598–1601.
[19] L. Bi, S.Q. Zhang, L. Zhang, Z.T. Tao, H.Q. Wang, W. Liu, Int. J. Hydrogen Energy 34 (2009) 2421–2425.
[20] F. Zhao, Q. Liu, S.W. Wang, K. Brinkman, F.L. Chen, Int. J. Hydrogen Energy 35 (2010) 4258–4263.
[21] K. Xie, R.Q. Yan, X.R. Chen, D.H. Dong, S.L. Wang, X.Q. Liu, G.Y. Meng, J. Alloy Compd 472 (2009) 551–555.
[22] K. Xie, R.Q. Yan, X.Q. Liu, J. Alloy Compd 479 (2009) L40–L42.
[23] Z.T. Tao, Z.W. Zhu, H.Q. Wang, W. Liu, J. Power Sources 195 (2010) 3481–3484.
[24] J.H. Tong, D. Clark, M. Hoban, R. O'Hayre, Solid State Ionics 181 (2010) 496–503.
[25] J.S. Park, J.H. Lee, H.W. Lee, B.K. Kim, Solid State Ionics 181 (2010) 163–167.
[26] N. Ito, H. Matsumoto, Y. Kawasaki, S. Okada, T. Ishihara, Solid State Ionics 179 (2008) 324–329.
[27] S. Imashuku, T. Uda, Y. Nose, G. Taniguchi, Y. Ito, Y. Awakura, J. Electrochem. Soc. 156 (1) (2009) B1–B8.
[28] A. Magraso, C. Frontera, A.E. Gunnæs, A. Tarancon, D. Marrero-López, T. Norby, R. Haugsrud, J. Power Sources 196 (2011) 9141–9147.
[29] A. Magraso, C. Kjølseth, R. Haugsrud, T. Norby, Int. J. Hydrogen Energy 37 (2012) 7962–7969.
[30] W.P. Sun, L.T. Yan, Z. Shi, Z.W. Zhu, W. Liu, J. Power Sources 195 (15) (2010) 4727–4730.
[31] R.D. Shannon, Acta Crystallogr. A32 (1976) 751–767.
[32] K.D. Kreuer, Solid State Ionics 125 (1999) 285–302.
[33] P. Babilo, T. Uda, S.M. Haile, J. Mater. Res. 22 (2007) 1322–1330.
[34] T. Scherban, Y.M. Baikov, E.K. Shalkova, Solid State Ionics 66 (1993) 159–164.
[35] A.S. Nowick, A.V. Vaysleyb, Solid State Ionics 97 (1997) 17–26.
[36] K.D. Kreuer, St. Adams, W. Munch, A. Fuchs, U. Klock, J. Maier, Solid State Ionics 145 (2001) 295–306.
[37] A. D'Epifanio, E. Fabbri, E.D. Bartolomeo, S. Licoccia, E. Traversa, Fuel Cells 8 (2008) 69–76.
[38] E. Fabbri, D. Pergolesi, A. D'Epifanio, E.D. Bartolomeo, G. Balestrino, S. Licoccia, E. Traversa, Energy Environ. Sci. 1 (2008) 355–359.
[39] C. Peng, J. Melnik, J.X. Li, J.L. Luo, A.R. Sanger, K.T. Chuang, J. Power Sources 190 (2009) 447–452.
[40] Z.Q. Sun, E. Fabbri, L. Bi, E. Traversa, Phys. Chem. Chem. Phys. 13 (2011) 7692–7700.
[41] L. Bi, E. Fabbri, Z.Q. Sun, E. Traversa, Energy Environ. Sci. 4 (2011) 1352–1357.